Investigation of the Near Wake of a Propfan

D. B. Hanson*
Hamilton Standard, Windsor Locks, Connecticut
and
W. P. Patrick†
United Technologies Research Center, East Hartford, Connecticut

The flow in the wake of a model single-rotation propfan rotor operating in a wind tunnel was traversed with a hot-wire anemometer system designed to determine the three periodic velocity components. Special data acquisition and data reduction methods were required to deal with the high data frequency, narrow wakes, and large fluctuating air angles in the tip-vortex region. The model-tip helical Mach number was 1.17, simulating the cruise condition. Although the velocity field is complex, flow features such as viscous velocity defects, vortex sheets, tip vortices, and propagating acoustic pulses are clearly identified with the aid of a simple analytical wake theory.

Introduction

PROPFAN wakes are of vital interest because they can impinge on downstream blades or structures causing noise and vibration. Furthermore, they contain considerable information relating to steady performance of the rotor. This work focuses on flow that is steady, but circumferentially nonuniform, in the coordinate system of the wake generating rotor. This would cause unsteady loading on the rear rotor of a counter-rotation propeller (CRP) due to the relative motion and is a major source of noise in CRPs. Circumferential averages of the velocity components are not addressed in detail herein as these are handled better by other theoretical and experimental methods.

A goal of the experiment was to resolve the fine structure of the wake and to compare it with predictions of an analytical model. It was anticipated that the widths of the viscous portion of the wakes could be as small as 1.2 mm (0.05 in.). This small scale and the high rpm (11,000) necessitated a data acquisition system with good response to frequencies well above 100,000 Hz. These requirements led to some unusual choices in measurement methods as will be described below. Blades tested were from the SR-3 propfan shown in Fig. 1. (A complete description of the model and its performance is given by Rohrbach et al.[1]) Because of power limitations in the model drive system, only two blades out of the eight were used for the hot-wire test. This turned out to be beneficial because wake overlap was minimized and the data were much easier to interpret. Furthermore, the tunnel Mach number was 0.32, far short of the design cruise Mach number of 0.8. This also was an advantage because the background flow seen by the hot wires was slow enough that compressibility did not have to be factored into the data acquisition and reduction methods.

The data described herein were acquired in 1978 but not reduced until later. At the time, there were no data known to the authors on time dependent wakes of propellers with supersonic tip speed. In 1981 Serafini et al.[2] reported results of using a laser Doppler velocimeter to measure the flowfield upstream and in the wake of the SR-3 model with the full set of blades at the actual Mach 0.8 design condition. Examination of Ref. 2 yields considerable information on the tip vortex but the viscous wake does not seem to have been resolved. With this as motivation, the 1978 data were reduced and then analyzed under contract to NASA Lewis Research Center as reported in Ref. 3.

Test Facilities

The wind tunnel used for this test was the Acoustic Research Tunnel at the United Technologies Research Center (UTRC) in East Hartford, Connecticut. The open-jet test section was run with a 42-in. diam. tunnel inlet nozzle. Total turbulence level in this facility is about 0.2%. A complete description of the facility is given in Ref. 4.

The propeller was driven by the 150-hp rig used for the original propfan model testing at UTRC.[6] A Task electric motor provided close speed control. Torque was measured establishing a power coefficient of 0.09 (93 shp), and a once-per-revolution signal was supplied as needed for data acquisition and reduction.

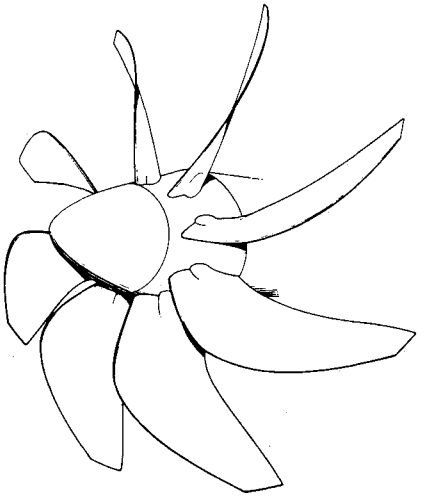

Fig. 1 SR-3 propfan.

Presented as Paper 89-1095 at the AIAA 12th Aeroacoustics Conference, San Antonio, TX, April 10-12, 1989; received June 6, 1989; revision received Nov. 15, 1989.

*Senior Principal Research Engineer. Associate Fellow AIAA.
†Lead Research Engineer. Member AIAA.

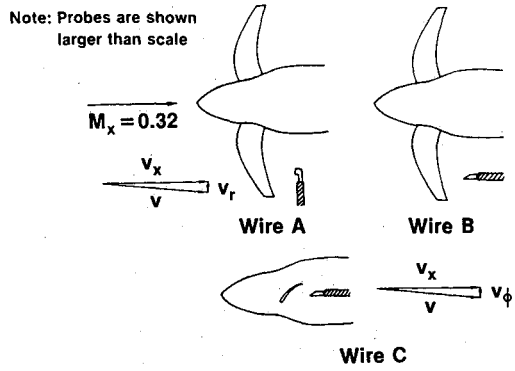

Fig. 2 Probe orientations for hot-wire measurements.

Wake Data Acquisition System

A hot-wire data acquisition and data reduction system was developed specifically for the study of the near wakes of high-speed turboprops. Wire active length was very small (0.064 cm) and frequency response was very high (350 kHz) to assure resolution of the fine structure including viscous wakes and the tip vortex. Near-wake data were obtained in a radial traverse one-half chord downstream from the propfan trailing edge at 10 stations between 60 and 102.5% of the propeller radius.

Hot-Wire Equipment

A TSI model 1050 constant-temperature anemometer with a 1:1 bridge and a 15-m probe cable was specially tuned by the manufacturer to provide the high-frequency response necessary to resolve the wake structure. The system frequency response was documented with the electronic square wave test to exceed 350 kHz when operated in the $M = 0.32$ stream with 0.00038-cm (0.00012-in.) diam, 0.064-cm (0.025-in.) long tungsten hot-wire sensors used in this test program.

Prong and wire-wake interference effects, which occur with conventional 3-wire probes, were avoided by taking consecutive measurements with three single-wire probes to obtain the three-dimensional velocity field. Laser assisted positioning of the hot-wire probes between tests ensured that the effective measurement volume was less than 0.1 cm.[3]

As shown in Fig. 2, three sensor orientations were chosen for measuring the 3 velocity components. In orientation A, the wire was aligned parallel to the radial direction. In orientation B, the wire was in the axial-radial plane at a 45-deg angle to both v_x and v_r. Finally, in orientation *C*, the wire was in the axial-azimuthal plane at a 45-deg angle to both v_x and v_ϕ. Wire orientations were chosen to maximize the hot-wire response to velocity perturbations anticipated in the propfan wake and to orient the prongs to preclude prong/wake interference effects.

Data Acquisition

The data required to determine the three-dimensional mean and periodic components downstream from the propfan at one radial station for one test condition were obtained in three runs, one for each wire orientation. The instantaneous hot-wire output voltage was sampled following a 1/rev trigger using a SAICOR correlator and probability analyzer for a time period equal to approximately two-thirds of a rotor rotation for 8192 consecutive revolutions. During the averaging period, rotor rpm was held constant to within 0.05%.

The sample data were ensemble averaged by the correlator to obtain signal enhanced periodic voltage traces that were output to an *X-Y* plotter (see Fig. 3) and were later entered into data files on an IBM PC using a digitizing pad. The digitized data files for wires A, B, and C, which contained data that had been digitized at random azimuth angles, were then processed and merged into a data file that contained voltages for each of the three wires at a common set of azimuth angles.

Errors in the voltage signal due to averaging over a finite (8192 member) ensemble and due to digitizing were less than $\pm 0.22\%$ and $\pm 0.20\%$ of the hot-wire voltage, respectively.

Data Reduction

As shown in Fig. 3, unlinearized hot-wire voltages were used as inputs into a computer program that used a Newton-Raphson iteration procedure to determine u, v, and w, the Cartesian velocity components in the laboratory frame, from hot-wire voltages E_{W_A}, E_{W_B}, E_{W_C}. The data reduction procedure incorporated the complete set of hot-wire response equations. No velocity component was assumed negligible, and no voltages were assumed to be small. This approach was necessary because the periodic variations in all three velocity components were significant. The program solved the following matrix formulation of the hot-wire response equations iteratively until δu, δv, and δw were minimized.

$$\begin{bmatrix} \frac{\partial F_A}{\partial u} & \frac{\partial F_A}{\partial v} & \frac{\partial F_A}{\partial w} \\ \frac{\partial F_B}{\partial u} & \frac{\partial F_B}{\partial v} & \frac{\partial F_B}{\partial w} \\ \frac{\partial F_C}{\partial u} & \frac{\partial F_C}{\partial v} & \frac{\partial F_C}{\partial w} \end{bmatrix} \begin{bmatrix} \delta u \\ \delta v \\ \delta w \end{bmatrix} = \begin{bmatrix} -F_A \\ -F_B \\ -F_C \end{bmatrix} \tag{1}$$

The functions F_A, F_B, and F_C are defined by the equations

$$F_A = U_A^2 - U_{A\text{eff}}^2 \tag{2}$$

$$F_B = U_B^2 - U_{B\text{eff}}^2 \tag{3}$$

$$F_C = U_C^2 - U_{C\text{eff}}^2 \tag{4}$$

where U_A, U_B, and U_C are the cooling velocities corresponding to hot-wire voltages E_{W_A}, E_{W_B}, and E_{W_C}, respectively.

To determine U_A, U_B, and U_C, the following version of King's Law

$$Nu = A + B(\rho U)^n \tag{5}$$

was used to characterize the heat transfer from each wire. Because the mean flow behind the propeller in the $M = 0.32$ freestream was assumed to be incompressible, Eq. (5) was expressed in the data reduction program in the following form

$$\left(\frac{E_W}{R_{\text{con}}}\right)^2 \left(\frac{R_w}{R_w - R_c}\right) = A' + B'\left(\frac{T_R}{T_0}U\right)^n \tag{6}$$

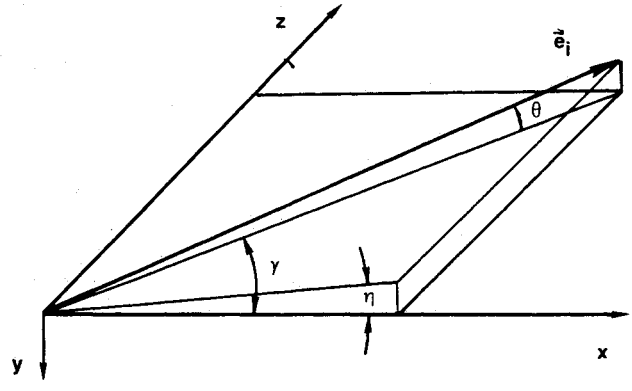

Fig. 3 Hot-wire coordinate system.

where R_w is the resistance of the heated wire, R_c the wire resistance at T_0, the wind-tunnel stagnation temperature, R_{con} the control resistance, and T_R the stagnation temperature of the calibration jet. This particular formulation was chosen because of anticipated large differences between T_R and T_0, which were uncontrollable in the atmospheric-intake wind tunnel. In actuality, because of moderate weather conditions T_R/T_0 varied less than $\pm 1.1\%$ throughout the test program.

The effective cooling velocities U_{eff} were assumed to follow the Champagne cosine law[7]

$$U_{\text{eff}}^2 = U_\perp^2 + k^2 U_\parallel^2 \tag{7}$$

where $U_\perp$ and $U_\parallel$ are the velocity components normal to and parallel to the hot-wire axis, respectively. Using Eq. (7) the effective cooling velocities for each wire can be derived in terms of the flow velocities u, v, and w to be

$$U_{A\text{eff}}^2 = u^2(\cos^2\gamma_A + k_A{}^2 \sin^2\gamma_A + v^2) + w^2(\sin^2\gamma_A + k_A{}^2\cos^2\gamma_A) - 2(1 - k_A{}^2)uv\sin\gamma_A\cos\gamma_A \tag{8}$$

$$U_{B\text{eff}}^2 = u^2 + v^2 + w^2 - (1 - k_B{}^2) \times (u\cos\theta_B\cos\gamma_B - v\sin\theta_B + w\cos\theta_B\sin\gamma_B)^2 \tag{9}$$

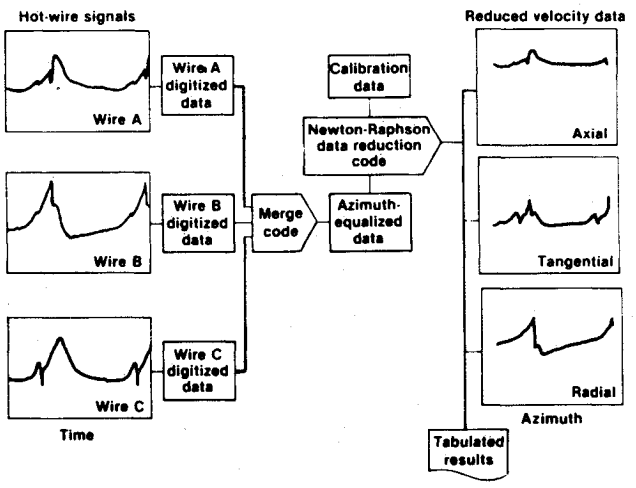

Fig. 4 Hot-wire data reduction procedure.

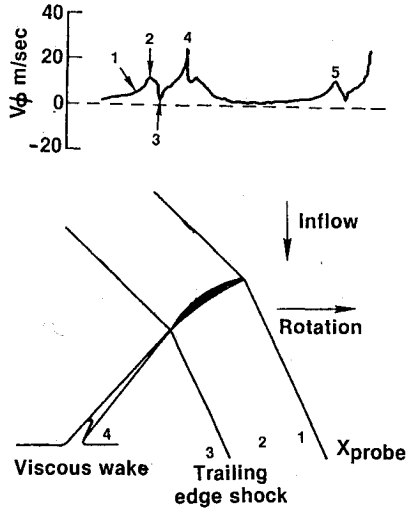

Fig. 5 Relation between blade-flow features and tangential velocity trace at $r/R = 0.9$.

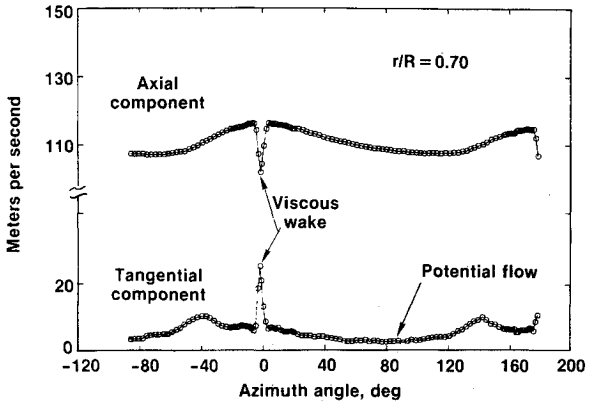

Fig. 6 Axial and tangential velocity traces at $r/R = 0.7$.

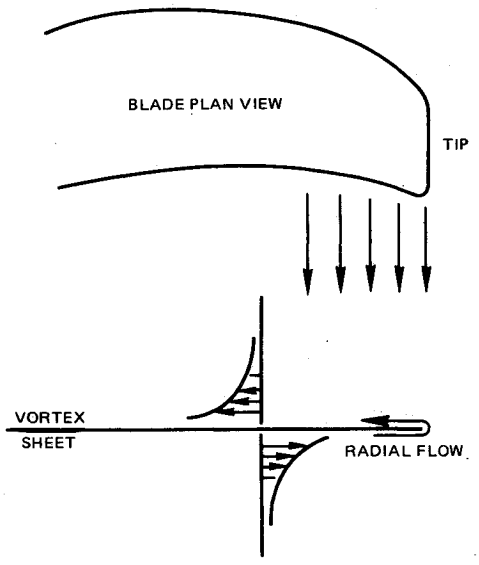

Fig. 7 Vortex sheet and radial flow.

$$U_{C\text{eff}}^2 = u^2 + v^2 + w^2 - (1 - k_C{}^2) \times (u\cos\theta_C\cos\eta_C - v\sin\theta_C + w\cos\theta_C\sin\eta_C)^2 \tag{10}$$

where wire angles γ, η, and θ are defined in Fig. 4. The u, v, and w velocity components obtained from the Newton-Raphson iteration procedure were converted to circumferential velocity components v_x, v_r, and v_ϕ using the transformations $v_x = u$, $v_r = -v$, $v_\phi = w$.

Estimates of Experimental Error

Experimental error limits were estimated following the technique developed by Tillman et al.[5] for a similar experimental setup. Separate error estimates were made for the potential flow and for the viscous wake regions. Error bounds were established for the repetitive (nonrandom) velocity components in the stationary frame. Relative to the flight speed V, errors in the fluctuating axial, radial, and tangential velocity components were ± 1.0, ± 2.9, and $\pm 0.7\%$, respectively, in the potential flow and 2.6, ± 3.0, and $\pm 1.2\%$, respectively, in the viscous portion of the wake.

Sample Results and Interpretation

Before presenting all of the test results, we show in this section sample data traces to illustrate some of the informa-

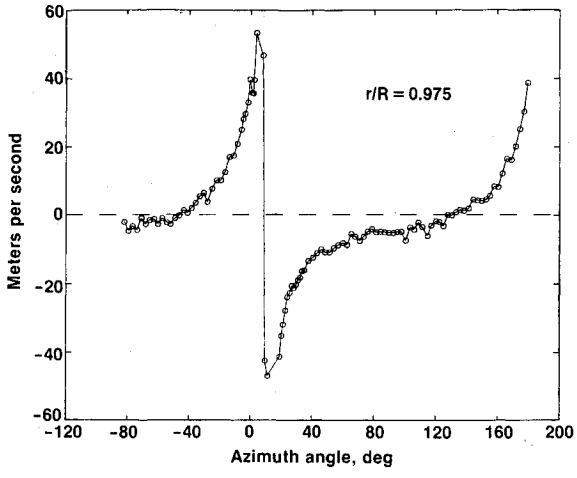

Fig. 8 Measured radial velocity component at $r/R = 0.975$.

tion present in the wakes. The following section describes the analytical wake model and then all of the data are presented in comparison with the theoretical predictions.

Figure 5a shows a typical plot of the tangential velocity component. Time on the abscissa corresponds to slightly more than a blade passing period. Numbers shown with the trace correspond to features in the field that can be understood on a two-dimensional basis using Fig. 5b. Consider the probe to be fixed in the flow as indicated by the X in the Fig. 5b. Also, consider the flowfield to be locked to the blade section and rotating with it. This flowfield would include 1) a bow shock; 2) a recovery region; and 3) a trailing shock, if the Mach number is high enough; and 4) a viscous wake. The flow pattern is dragged past the probe in the rotation direction so that the wake events are observed in the order shown. The shock waves are felt first; however, for this operating condition, the bow shock (which would be at location 1) is suppressed by leading-edge sweep, i.e., the section relative Mach number times the cosine of the leading-edge sweep angle is less than unity. There is, however, a pulse from the midchord area at location 2, and a trailing-edge shock is clearly seen at location 3. In fact, the pulse in the 1-3 area looks very much like a noise pulse as measured by a microphone for this condition and reported, for example, in Ref. 6. The viscous wake produces the peak in the trace at location 4. The number 5 on the trace at the right indicates the beginning of the wake from the next blade.

Figure 6, which shows the axial and tangential components at radius ratio 0.7, can be used to explain sign conventions. The plots show clearly divided regions of viscous and potential flow. For the axial component, the velocity is positive in the downstream direction. Thus, the viscous wakes, which are at the vortex sheets, represent retarded flow. The potential contribution is positive at the vortex sheets, representing a downstream impulse. This illustrates one of the difficulties in wake prediction, namely that the viscous and potential effects are opposed for the axial component so that partial cancellation is predicted. In the tangential component shown at the bottom in Fig. 6, positive values correspond to components in the direction of rotor rotation. Thus, in the viscous region, the blade drags the wake flow in the direction of rotation, and the potential flow imparts an impulse in the same direction.

As was just shown, much of the axial and tangential flow is explainable in two-dimensional terms. However, the radial velocity component is exclusively a three-dimensional effect and is discussed with reference to Fig. 7. The planform at the top could represent either a wing or a propeller blade. The variation of the loading, or circulation, along the span produces the trailing vortex system. In fact, if Γ is the circulation at any radius r, then the strength of the trailing vorticity at that radius is proportional to $\partial\Gamma/\partial r$. Because the circulation drops very rapidly to zero at the tip, the vorticity is strongest there. The vortex sheet is a slip surface. Underneath the sheet, on the side corresponding to the pressure side of the blade, the flow near the tip is radially outward and above the sheet it is radially inward. In simple terms, the flow leaks around the tip from the pressure side to the suction side. At the sheet, there is a velocity jump of the form suggested at the bottom in Fig. 7. This characteristic jump does occur in the data as shown by the sample trace in Fig. 8. The sign of the jump is, of course, given by the sign of $\partial\Gamma/\partial r$. At the point along the span where the circulation has its maximum value, $\partial\Gamma/\partial r$ changes sign providing a powerful diagnostic tool for checking loading distributions.

Analytical Wake Model

A wake prediction method based on Hanson's helicoidal lifting surface theory[8] can be used to help interpret the wake waveforms in terms of source mechanisms. This is a linear acceleration potential procedure in which the far wake appears as a nested set of helicoidal vortex sheets and the near-field effects appear as the compressible field of source and doublet distributions corresponding to the blade thickness and loading. Viscous wake velocity defects are patched in via the two-dimensional formulas of Silverstein et al.[9] The theory is only outlined below; details can be found in the references.

The basis of the theory is the linear wave equation for the disturbance pressure p

$$\nabla^2 p - \frac{1}{c_0^2}\frac{\partial^2 p}{\partial t^2} = -\rho_0 \frac{\partial q}{\partial t} + \nabla \cdot f \tag{11}$$

where c_0 is the ambient density and t the time. Action of the blade thickness and loading is accounted for by motion of a source distribution q and a body force f on helicoidal surfaces. For convenience, forward flight is represented by helical motion of the sources with the static wave equation rather than by circular motion with the convected wave equation.

As shown in Ref. 8, Eq. (11) is developed into an acceleration potential and then a velocity potential using classical methods. Differentiating the potential gives the downwash in terms of the unknown loading; the loading, in turn, is found by discretizing the downwash equation and inverting. With the thickness and the computed loading, the potential equation gives the entire flowfield.

The equation for the potential Φ follows immediately from Ref. 8 and can be written in the following form.

$$\Phi = \Phi_{LI} + \Phi_{LC} + \Phi_T \tag{12}$$

where the subscript LI denotes the incompressible loading term, LC the compressible loading term, and T the thickness term. The potential terms are shown below.

$$\Phi_{LI} = \frac{iB}{8\pi V^2}\int_{root}^{tip} \frac{bU_0^3 C_L}{r_0} \times \sum_{m=-\infty}^{\infty} n e^{in\phi} I_n\left[\frac{|n|\Omega r_<}{V}\right] K_n\left[\frac{|n|\Omega r_<}{V}\right] dr_0 \tag{13}$$

$$\Phi_{LC} = \frac{iB}{16\pi V^2}\int_{root}^{tip} \frac{U_0}{r_0}\sum_{m=-\infty}^{\infty} e^{in\phi} \times \int_{-\infty}^{\infty}\int_{L.E.}^{T.E.} \Delta C_p(\gamma_0) e^{i\omega\gamma_0/U_0} d\gamma_0 \times \frac{1}{\omega}\left[\Omega r_0^2(\omega - n\Omega) - nV^2\right] \times J_n(\mu r_<) H_n^{(1)}(\mu r_>) e^{-i\omega x/V} d\omega\, dr_0 \tag{14}$$

$$\Phi_T = \frac{-B}{8\pi V}\int_{root}^{tip}\sum_{m=-\infty}^{\infty} e^{in\phi} \times \int_{-\infty}^{\infty}\int_{L.E.}^{T.E.} h(\gamma_0)e^{i\omega\gamma_0/U_0}\,d\gamma_0 \times \omega J_n(\mu r_<)H_n^{(1)}(\mu r_>)e^{i\omega x/V}\,d\omega\,dr_0 \tag{15}$$

where the harmonic index $n = mB$ and the radial wave number

$$\mu = \sqrt{\left(\frac{\omega}{c_0}\right)^2 - \left(\frac{\omega - n\Omega}{V}\right)^2} \tag{16}$$

In the preceding, the field point in cylindrical coordinates is r, ϕ, x. Also, B, V, b, and Ω are the number of blades, flight speed, chord, and angular speed, respectively. r_o and γ_o are radial and chordwise distance on the blade, and the notation $r_<$, $r_>$ implies the lesser, greater r and r_o. C_L and ΔC_p are coefficients of section lift and lift pressure. Finally, I_n, K_n, J_n, and $H_n^{(1)}$ are standard Bessel functions and $i^2 = -1$.

Velocity components discussed below are found by operating on the potential as follows

$$v_x = \frac{\partial\Phi}{\partial x}, \qquad v_r = \frac{\partial\Phi}{\partial r}, \qquad v_\phi = \frac{1}{r}\frac{\partial\Phi}{\partial\phi} \tag{17}$$

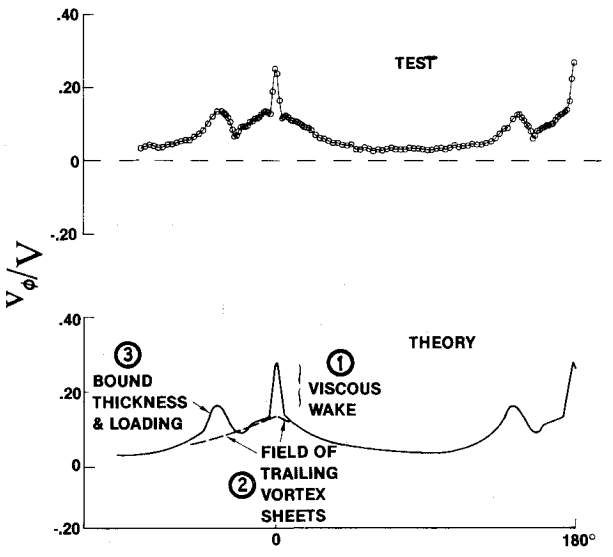

Fig. 9 The three components of the wake theory (at $r/R = 0.85$).

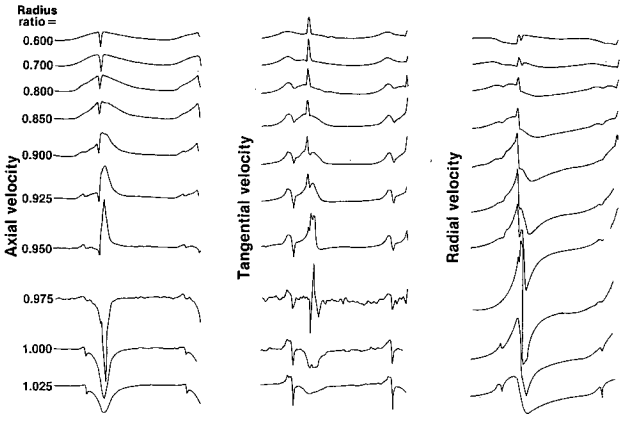

Fig. 10 Composite of all wake data.

For the ensuing discussions, it is convenient to express the load contributions as the sum of a wake term and a near-field term as follows

$$\Phi_W = 2\Phi_{LI}, \qquad \Phi_N = \Phi_{LC} - \Phi_{LI} \tag{18}$$

These can be distinguished easily in Fig. 9 where the wake term Φ_W, labeled with a 2, is the smoothly varying once per blade component.

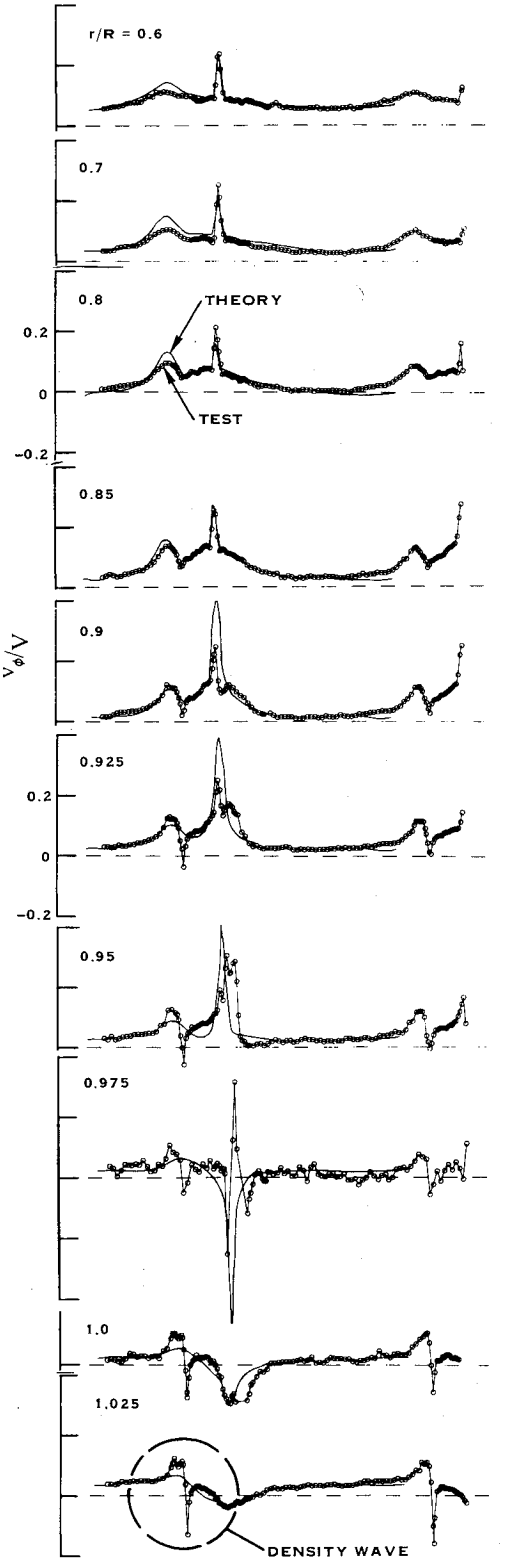

Fig. 11 Tangential velocity component—test and theory.

This term was discussed previously as a cause of noise in counter-rotation propellers.[10] It is incompressible and extends, in theory, to downstream infinity. The near-field term Φ_N, labeled with a 3, contains the compressibility effect through the finite speed of sound c_0. This was programmed recently,[3] and results are shown here for the first time. The viscous wake, labeled with a 1, is placed at the vortex sheet.

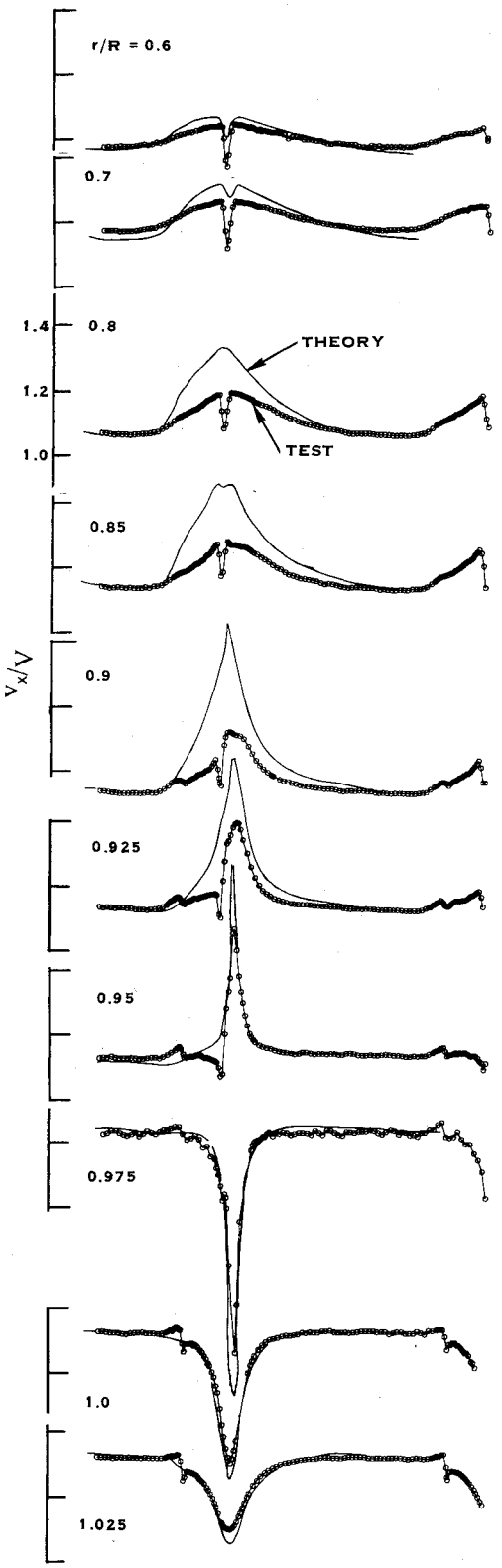

Fig. 12 Axial velocity component—test and theory.

Test/Theory Comparison

Prepared by the physical discussion and analytical model of the preceding two sections, we now examine the remainder of the data. Figure 10 shows all of the experimental results: three velocity components at 10 stations along a radial line passing through a point 0.5 chord axially downstream from the tip trailing edge. As would be expected, the disturbances are most violent in the tip area. The axial and tangential components there are strong and local as opposed to their weaker, more spread-out character at $r/R = 0.6$. In the axial velocity traces, the sign of the potential flow pulse changes between $r/R = 0.95$ and 0.975 indicating that the tip vortex lies between these two radii. This sign change seems to be a very reliable locator for the vortex and was used online for guidance during the tests. The radial velocity component at the right in Fig. 10 exhibits the jump linked above to the variation in circulation. At $r/R = 0.7$ the sign of the jump changes indicating that the circulation peak is near that radius. Figures 11–13 show the theory/data comparisons for the three velocity components. In generating these figures, certain liberties were taken that must be explained. First, the theory curves were shifted horizontally and vertically for the best fit. The vertical shift was applied because the blockage of the centerbody, which produces axial and radial offsets in the mean flow, is not included in the theory. The mean value of the tangential component was very difficult to measure accurately because of critical dependence on probe alignment. The horizontal shift was applied because distortion due to swirl also is not included in the analysis. Finally, the analysis does not recognize contraction of the slipstream behind the rotor so that the tip of the theoretical vortex sheet always lies at $r/R = 1$. To compensate for this, the radial stations calculated were adjusted so that the tip flow fell between the $r/R = 0.95$ and 0.975 stations as required by the change of sign in axial component shown in Fig. 10. All of the stations were adjusted to give the same percentage change in annular area as the tip station according to Table 1.

Tangential velocity predictions are shown first in Fig. 11. They are seen to agree well with data over the entire radial range. In particular, the split between viscous and potential effects and between bound and trailing effects is well represented. In reducing the data at $r/R = 0.975$, convergence difficulties were encountered in the data reduction program so that this trace probably includes some extra uncertainty. At the outer radii, the predicted pulse associated with bound effects does not have the strength or sharpness of the data trace. At first this was believed to be a failure of the velocity predictions, but further thinking suggests that the wire voltage is responding to density as well as velocity waves. The data acquisition and reduction scheme was designed assuming incompressible flow. This was done because the mean flow over the hot-wire probes is basically the tunnel speed ($M = 0.32$) plus the small amount of axial induction. Hot wires respond to ρu [Eq. (5)], which in incompressible flow varies only with velocity. However, the acoustic pulse is a density wave that influences this portion of the data trace. Analysis of data from microphones very near the blade tips[6] indicates pressure variations large enough to explain the pulse circled for r/R in Fig. 11.

Figure 12 compares the predicted and measured axial velocity components. At inboard radii, it can be seen for this component that the viscous wake is underpredicted. Because the vector sum of the axial and tangential components is

Table 1 Radial stations

Data	Calc	Data	Calc
0.600	0.616	0.925	0.954
0.700	0.720	0.950	0.979
0.800	0.824	0.975	1.005
0.850	0.876	1.000	1.031
0.900	0.927	1.025	1.060

approximately correct, the error may be due to neglect of changes in flow direction induced by rotor loading. Also, at radius ratios from 0.8 to 0.9, the potential velocity pulse is predicted to be much stronger than the test indicates. The reason for this has not yet been established but could also be associated with angle changes in the mean flow. However, in the tip area (outboard of 92.5% radius), the agreement is very satisfying, particularly regarding the flip in sign of the velocity pulse at the tip vortex.

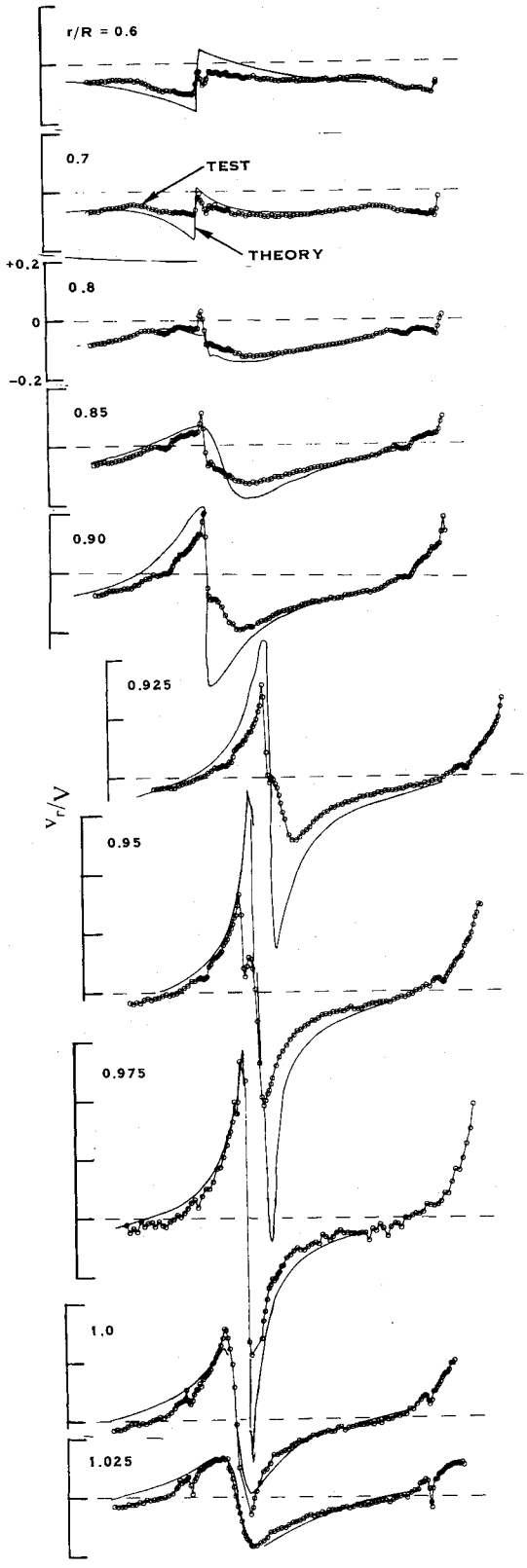

Fig. 13 Radial velocity component – test and theory.

Finally, Fig. 13 gives the comparisons for the radial velocity component. Again the general characteristics are well predicted, particularly in the tip area. The major discrepancies are at the inner radii where the magnitude of the velocity jump is overpredicted. The change in the sign of the velocity jump is predicted to occur slightly outboard of that for the data. This suggests that the loading distribution may not be quite correct. There seems to be some radial viscous flow shed from the blade boundary layer. This effect is not included in the theoretical model. At $r/R = 0.90$ and 0.925 the negative part of the pulse after the jump is not correctly predicted. A separate analysis suggests that this is caused by rollup of the wake, which is currently neglected in the theory.

Concluding Remarks

A hot-wire system has been developed for measurement of flow in the wake of a model propfan operating at supersonic tip speed. The constant-temperature anemometer system with a 350-kHz frequency response permitted wake structures as fine as 0.035 cm to be resolved. Phase-averaged axial, radial, and tangential velocity data were obtained for a complete blade passage at 10 radial stations located one-half chord downstream from the propfan trailing edge. Obtaining the data with three single-wire probes avoided interference with the wake of the probe wire support prong frequently encountered with conventional 3-wire probes.

An analytical model for the wake that includes the effects of the trailing helicoidal system of vortex sheets, the bound potential thickness and loading effects, and a two-dimensional representation of the viscous wake velocity defects was presented. With the help of this model, each of these effects is clearly identified in the test data.

Acknowledgments

This work was supported by NASA Lewis Contract NAS3-23720 and by independent research and development funding from United Technologies Research Center and Hamilton Standard.

References

[1]Rohrbach, C., Metzger, F. B., Black, D. M., and Ladden, R. M., "Evaluation of Wind Tunnel Performance Testings of an Advanced 45 deg Swept Eight Bladed Propeller at Mach Numbers From 0.45 to 0.85," NASA Contractor Rept. 3505, March 1982.

[2]Serafini, J. S., Sullivan, J.P., and Neumann, H. E., "Laser-Velocimeter Flow-Field Measurements of an Advanced Turboprop," NACA TM-82677, 1981.

[3]Hanson, D. B., McColgan, C. J., Ladden, R. M., and Klatte, R. J., "Unified Aeroacoustics Analysis for High Speed Turboprop Aerodynamics and Noise," Vol. III, final report (draft) under Contract NAS3-23720, 1988.

[4]Paterson, R. W., Vogt, P. G., and Foley, W. M., "Design and Development of the United Aircraft Research Laboratories Acoustic Research Tunnel," *Journal of Aircraft,* Vol. 20, No. 7, 1973, pp. 427–433.

[5]Tillman, T. G., Simonich, J. C., and Wagner, J. H., "Hot Wire Measurements Downstream of a Prop-Fan," AIAA Paper 89-2698, 1989.

[6]Brooks, B. M., "Acoustic Measurement of Three Prop-Fan Models," AIAA Paper 80-0995, 1980.

[7]Champagne, F. H., Sliecher, C. A., and Wehrmann, O. H., "Turbulence Measurements with Inclined Hot-wires, Part. 1. Heat Transfer Experiments with Inclined Hot-wires," *Journal of Fluid Mechanics,* Vol. 28, Pt. 1, 1967, pp. 153–175.

[8]Hanson, D. B., "Compressible Helicoidal Surface Theory for Propeller Aerodynamics and Noise," *AIAA Journal,* Vol. 21, No. 6, 1983, pp. 19–27.

[9]Silverstein, A., Katzoff, S., and Bullivant, W. K., "Downwash and Wake Flow Behind Plain and Flapped Airfoils," NACA TR-651, 1939.

[10]Hanson, D. B., "Noise of Counter-Rotation Propellers," *Journal of Aircraft,* Vol. 22, No. 7, 1985, pp. 609–617.